

# A Novel Robust Model Reference Adaptive Impedance Control Scheme for an Active Transtibial Prosthesis

Siamak Heidarzadeh, Mojtaba Sharifi, Hassan Salarieh\* and Aria Alasty

*School of Mechanical Engineering, Sharif University of Technology, P.O. Box: 11155-9567, Tehran, Iran*

*E-mails: [heidarzadehsiamak@yahoo.com](mailto:heidarzadehsiamak@yahoo.com), [mojtaba\\_sharifi@mech.sharif.edu](mailto:mojtaba_sharifi@mech.sharif.edu), [salarieh@sharif.edu](mailto:salarieh@sharif.edu), [aalasti@sharif.edu](mailto:aalasti@sharif.edu)*

(Accepted January 19, 2019. First published online: March 12, 2019)

## SUMMARY

In this paper, a novel robust model reference adaptive impedance control (RMRAIC) scheme is presented for an active transtibial ankle prosthesis. The controller makes the closed loop dynamics of the prosthesis similar to a reference impedance model and provides asymptotic tracking of the response trajectory of this impedance model. The interactions between human and prosthesis are taken into account by designing a second-order reference impedance model. The proposed controller is robust against parametric uncertainties in the nonlinear dynamic model of the prosthesis. Also, the controller has robustness against bounded uncertainties due to unavailable ground reaction forces and unmeasurable feedbacks of accelerations at the socket place. Moreover, an appropriate Series Elastic Actuator (SEA) mechanism for the prosthetic ankle is included in this work and its effects are discussed. Tracking performance and stability of the closed-loop system are proven via the Lyapunov stability analysis. Using simulations on an overall amputee prosthetic foot system, the effectiveness of the proposed RMRAIC controller is investigated for the task of level ground walking.

**KEYWORDS:** Ankle prosthesis; Physical human–robot interaction; Impedance control; Model reference adaptive control; Robust control.

## 1. Introduction

Lower-limb amputees usually experience reduced mobility and considerable disabilities compared with their non-amputee counterparts. Although passive prostheses are of interest to many researchers in this field,<sup>1,2</sup> amputees using these passive prostheses usually experience reduced walking performance including non-symmetric gait patterns and increased metabolic energy consumption.<sup>3–5</sup>

As a remedy to these shortcomings, powered ankle-foot prostheses have been designed and studied in recent years to improve the quality of life for amputees.<sup>6–10</sup> These active prostheses have been developed to replicate biomechanical characteristics of a human ankle and reduce the metabolic energy consumption during ambulation.

By evaluating available transtibial prostheses, the current challenge is to develop efficient and smart controllers because the mechanical systems in many cases have been satisfactorily designed.<sup>7,11,12</sup> Au et al.<sup>6,12</sup> developed an active powered ankle prosthesis with one degree of freedom (DOF) in the sagittal plane. Bellman et al.<sup>7</sup> designed an active robotic ankle prosthesis with two actuated DOF in the sagittal and coronal planes. In ref. [13], a high-performance ankle prosthetic emulator system was developed that had a suitable performance in human locomotion experiments.

\* Corresponding author. E-mail: [salarieh@sharif.ir](mailto:salarieh@sharif.ir)

The main concern in designing every control scheme for a transtibial prosthesis is the capability of replicating the normal human ankle functionality. Normal human ankle characteristics (i.e., stiffness, damping, etc.) change during each gait cycle and also at different walking speeds.<sup>14,15</sup> Thus, in order to replicate the behavior of a non-amputee human ankle, the prosthesis should be capable of controlling the joint impedance and position required in each task.

The idea of powered ankle-foot prosthesis was brought to light in the late 1990s.<sup>16</sup> Since then, the control of powered ankle-foot prostheses has been an interesting topic in the field of biomedical engineering. Au et al.<sup>17</sup> have used the finite state control scheme to control a powered ankle-foot prosthesis. They used SEA in the design of prosthesis to include elasticity in the mechanism.<sup>18,19</sup>

Holgate et al.<sup>20</sup> used phase plane control in order to control a 2-DOF transtibial ankle prosthesis. Their designed prosthesis had 1 DOF in the sagittal plane and 1 DOF in the coronal plane,<sup>7</sup> and each DOF was actuated with a robotic tendon.<sup>21</sup>

Recently, Yuan et al.<sup>22</sup> employed finite state control scheme for a 2-DOF ankle-and-toe mechanism designed for transtibial amputees.<sup>23</sup> A SEA mechanism has been used in their design,<sup>19,24</sup> which has 2 DOF, one at the ankle joint and the other at the toe.<sup>23</sup>

In most of the previous studies performed on the design and control of powered transtibial prostheses, researchers have used the SEA<sup>18,19</sup> or robotic tendon<sup>21</sup> in their design of mechanisms, to replicate the functions of able-bodied human ankle tendons and muscles. Both the SEA and robotic tendon comprised of a DC motor in series with a spring structure through a mechanical transmission. These mechanisms are intended to benefit from their inherent elasticity in order to reduce both peak power and energy requirements for the actuators,<sup>21</sup> and absorb the shock forces due to heel strike (HS) of the prosthesis with the ground.<sup>6</sup> In fact, one of the most hindering difficulties that arise in the control of an ankle prosthesis is the presence of these shock and impact forces at HS.<sup>6</sup>

It is necessary for the controller of a prosthesis to be flexible with respect to interaction forces of heel strike. Accordingly, the main reason for employing the SEA is to provide this flexible performance. However, in addition to utilizing a SEA-based mechanism, the effects of these impact forces should also be considered in the controller design. Impedance control is a suitable approach to realize a flexible human–robot interaction.<sup>25</sup> The impedance control theory has been utilized and justified by many researchers for most of the rehabilitation robots/devices.<sup>6,8,26</sup>

Although the mentioned control schemes<sup>17,20,22</sup> have shown appropriate performance, there has been no stability analysis attributed to these controller designs. In fact, most of the developed control laws that exist in the literature have used PD-like control structures. The main reason that the researchers are interested in these types of controllers is the minor sensory information required for the implementation of such control schemes. In other words, the ankle angle, angular velocity, and ground reaction forces (GRFs) are usually the only required sensory information for such schemes.<sup>17,20,22</sup> In contrast, to propose stable control laws based on the prosthetic model, additional sensory information (such as amputee–prosthesis interaction [API] forces and moment and/or accelerations at the amputated place) is usually required to implement such schemes. This is the main reason that simple PD-like control methods were suggested and used instead of stable nonlinear control schemes.

Some of the abovementioned issues have been considered and resolved in ref. [27], where an artificial neural network-based controller has been proposed in order to adaptively compensate for unmodeled dynamics and disturbances of the system and provide closed-loop stability.<sup>27</sup> However, they have neglected to include the impedance characteristics of walking in the design of the control system,<sup>27</sup> and no flexible mechanism has been included in their design. In another work, Azimi et al.<sup>28</sup> have designed a robust model reference adaptive impedance control (RMRAIC) scheme for an active knee prosthesis. In that work, the control scheme was designed for the knee joint and the amputated place simultaneously. Accordingly, full feedback of state variables is required to implement the control law.<sup>28</sup> Though the design in ref. [28] is promising, a shortcoming of the developed controller is the isolation of control scheme and the reference impedance model. Based on the above discussion, the main contributions of this research work can be summarized as follows:

- A new RMRAIC scheme is presented using a combination of robust control, impedance control, and model reference adaptive control (MRAC).
- In this design, accelerations, GRFs, position, and velocity of the amputated place are not required to be measured and used in the control law.

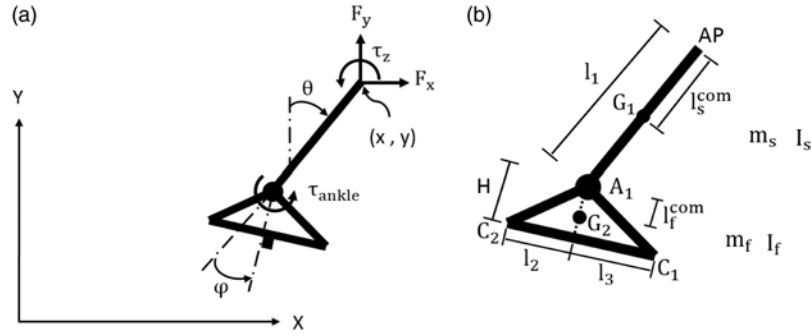


Fig. 1. Illustration of the employed ankle prosthesis model: (a) the coordinate system, kinematic variables, and positive angular directions, and (b) the geometrical and inertial parameters.

- The robustness of this controller is proved against parametric uncertainties, unknown accelerations, and GRFs using the Lyapunov method.
- The controller employs the parameters of a stable reference impedance model in its structure and makes the closed-loop dynamics of the prosthesis similar to the reference impedance model. Thus, the controller and the impedance model are not separated in the proposed strategy.
- A Series Elastic Actuator (SEA) is utilized in the design of prosthetic mechanism to reduce the effect of shock forces.

The stability of closed-loop system is proven using the Lyapunov stability analysis. Finally, the implementation of the proposed controller is evaluated using some simulations on an overall amputee–prosthetic foot system for the task of level ground walking.

The rest of this paper is organized as follows. In Section 2, the dynamic equations of the ankle prosthesis are formulated. Section 3 is devoted to designing a suitable RMRAIC law for the prosthetic system. In Section 4, the results of numerical simulations are presented to show the effectiveness of the proposed control algorithm. Conclusion is drawn in Section 5. Note that throughout this paper boldfaced and non-italicized letters are used for the vectors and matrices, while non-boldfaced and italicized letters are adopted for the scalars.

## 2. Dynamics of the Prosthetic Ankle Joint

### 2.1. Prosthetic dynamic modeling

Figure 1 shows the link segment representation of the ankle prosthesis in the sagittal plane where most of the ankle joint movements occur during a gait cycle. The dynamics of the prosthesis is derived using the Euler–Lagrange method, which is formulated as:

$$\mathbf{D}(\mathbf{q}) \ddot{\mathbf{q}} + \mathbf{C}(\mathbf{q}, \dot{\mathbf{q}}) \dot{\mathbf{q}} + \mathbf{G}_g(\mathbf{q}) + \mathbf{G}_e(\mathbf{q}) = \boldsymbol{\tau} + \mathbf{J}^T \mathbf{F}_e \quad (1)$$

where  $\mathbf{q} = [x \ y \ \theta \ \varphi]^T$  represents the position vector of the prosthetic ankle model;  $\mathbf{D}(\mathbf{q}) \in \mathbb{R}^{4 \times 4}$  is the mass matrix;  $\mathbf{C}(\mathbf{q}, \dot{\mathbf{q}}) \dot{\mathbf{q}}$  comprises the Coriolis and centrifugal term, where  $\mathbf{C}(\mathbf{q}, \dot{\mathbf{q}}) \in \mathbb{R}^{4 \times 4}$ ;  $\mathbf{G}_g(\mathbf{q}) \in \mathbb{R}^4$  and  $\mathbf{G}_e(\mathbf{q}) \in \mathbb{R}^4$  are the vectors of generalized forces associated with the gravitational forces, and the added elasticity of mechanism in dorsiflexion portion of the gait where the spring with tuned constant stiffness  $K_p^r$  bears the weight of human body,<sup>6</sup> respectively.  $\boldsymbol{\tau} \in \mathbb{R}^4$  represents a vector whose first three elements are the interaction forces and moment between the prosthesis and the amputee, and the last element is the control input torque  $\tau_{\text{ankle}}$ , given by:

$$\boldsymbol{\tau} = [F_x \ F_y \ \tau_z \ \tau_{\text{ankle}}]^T \quad (2)$$

Also  $\mathbf{J}^T \mathbf{F}_e \in \mathbb{R}^4$  in Eq. (1) denotes the vector of generalized torques generated by the GRFs shown in Fig. 2. In Fig. 1,  $l_1$  is the length of amputated shank,  $H$  is the total foot height,  $l_2$  is the distance from heel to the projection of foot center of mass on the foot bottom, and  $l_3$  is the distance from the projection of foot center of mass on the foot bottom to the toe. As an inertial parameter,  $I_s^{\text{com}}$  represents the location of the amputated shank center of mass from amputation place (AP).  $m_s$  and  $I_s$  denote the mass and rotational inertia of the amputated shank, respectively. Moreover,  $I_f^{\text{com}}$  is

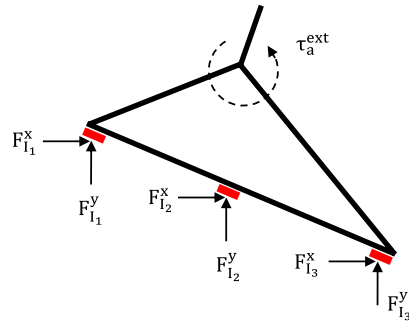


Fig. 2. Ground reaction forces measured at three different places beneath the prosthetic foot.

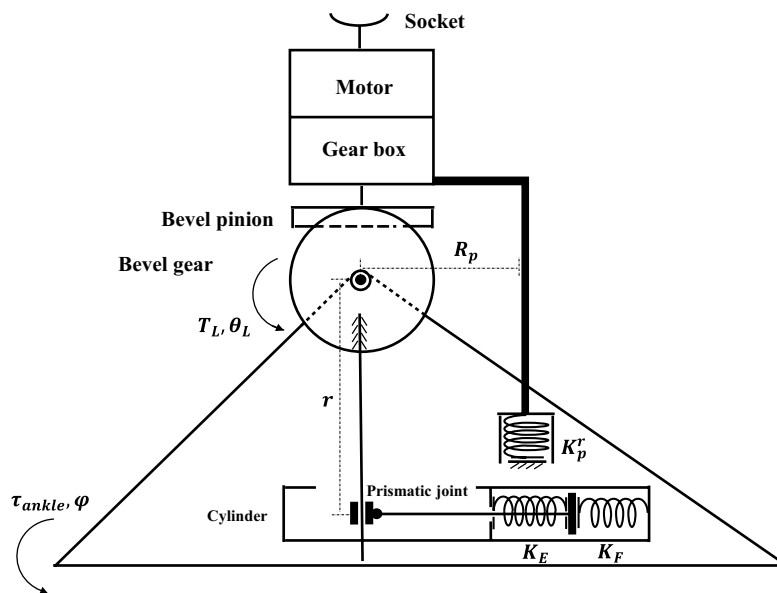


Fig. 3. The mechanism of ankle prosthesis.

the location of foot center of mass from the ankle joint ( $A_1$ ).  $m_f$  and  $I_f$  also denote the mass and rotational inertia of the foot, respectively.

The matrices in Eq. (1) have the following properties:

**Property 1.** The inertia matrix  $\mathbf{D}(\mathbf{q})$  is symmetric and positive definite.<sup>29–31</sup>

**Property 2.** The matrix  $\mathbf{C}(\mathbf{q}, \dot{\mathbf{q}})$  can be derived in such a way that  $\dot{\mathbf{D}}(\mathbf{q}, \dot{\mathbf{q}}) - 2\mathbf{C}(\mathbf{q}, \dot{\mathbf{q}})$  is skew symmetric.<sup>29,30,32</sup>

**Property 3.** For the arbitrarily selected signals  $\mathbf{v}_1 \in \mathbb{R}^4$  and  $\mathbf{v} \in \mathbb{R}^4$ , the left-hand side of Eq. (1) can be linearly parameterized in terms of the prosthetic model's unknown parameters as follows [29]:

$$\mathbf{D}(\mathbf{q}) \mathbf{v}_1 + \mathbf{C}(\mathbf{q}, \dot{\mathbf{q}}) \mathbf{v} + \mathbf{G}_g(\mathbf{q}) = \mathbf{Y}(\mathbf{q}, \dot{\mathbf{q}}, \mathbf{v}_1, \mathbf{v}) \boldsymbol{\theta}_a \quad (3)$$

where  $\boldsymbol{\theta}_a \in \mathbb{R}^p$  contains the unknown parameters of the prosthesis. Also the regressor matrix  $\mathbf{Y} \in \mathbb{R}^{4 \times p}$  contains known functions corresponding to the prosthetic dynamics.

Property 3 is useful in real situations, where the exact values of the inertial parameters  $I_s^{\text{com}}$ ,  $m_s$ ,  $I_s$ ,  $I_f^{\text{com}}$ ,  $m_f$ , and  $I_f$  are not known and only nominal values of these parameters are available. Moreover, it is a reasonable assumption that these unknown parameters have constant values.

## 2.2. Mechanism of the ankle prosthesis

Figure 3 shows the mechanism of the ankle prosthesis, which is a SEA similar to the standard SEA model adopted in ref. [18]. In this mechanism, the spring with constant stiffness  $K_p^r$  is included to

bear the weight of the human body during dorsiflexion phase of the gait cycle and to prevent damages to the prosthetic motor and transmission.<sup>6</sup> The function of this SEA mechanism is as follows: the motor's rotational motion is transferred to the bevel gear through the gear box and bevel pinion. The rotational motion of the bevel gear is converted to the linear motion of the slider in the cylinder via the prismatic joint. Compression of the extension/flexion spring  $K_E/K_F$  in the cylinder, which is permanently attached to the prosthetic foot, produces a clockwise/counterclockwise torque that causes ankle plantarflexion/dorsiflexion. Since the prosthetic ankle must be capable of providing high torque bandwidth and power output,<sup>6</sup> highly efficient electric motor should be chosen for the mechanism. As a result of this characteristic, the fast dynamics of the electric motor can be neglected and the following relation is obtained:

$$T_m = \frac{T_L}{\eta N} \quad (4)$$

where  $T_m$  is the motor torque,  $N$  is the total transmission ratio of gear box and bevel pinion and gear,  $\eta$  is the total efficiency of motor and its torque transmission, and  $T_L$  is the output torque of bevel gear.  $\theta_L$  is the rotation of bevel gear given by:

$$\theta_L = \frac{\theta_m}{N} \quad (5)$$

where  $\theta_m$  is the rotation of electric motor axis.

Due to the definitions of  $\tau_{\text{ankle}}$  and  $\theta_L$ , and the series springs in the mechanism, the relation between motor torque  $T_m$  and  $\tau_{\text{ankle}}$  can be written as:

$$T_m = \frac{1}{\eta N} (\tau_{\text{ankle}} + K_s r^2 \tan(\theta_L - \varphi)) \quad (6)$$

where

$$K_s = \begin{cases} K_F, & \theta_L \geq \varphi \\ K_E, & \theta_L < \varphi \end{cases} \quad (7)$$

The second term in the right-hand side of Eq. (6) can be defined as:

$$T_{SSE} = \frac{1}{\eta N} K_s r^2 \tan(\theta_L - \varphi) \quad (8)$$

where  $T_{SSE}$  denotes the series spring effect torque. In addition, when there exists no series spring in the mechanism, the bevel gear output torque  $T_L$  is equal to  $\tau_{\text{ankle}}$  and therefore the required torque by the motor in the absence of any series elasticity can be expressed as follows:

$$T_m^{NSE} = \frac{1}{\eta N} \tau_{\text{ankle}} \quad (9)$$

where  $T_m^{NSE}$  stands for the motor torque in the case of no series elasticity. Equations (8) and (9) together with Eq. (6) imply that:

$$T_m = T_m^{NSE} + T_{SSE} \quad (10)$$

which highlights the effect of the series springs in the mechanism.

### 3. Control

#### 3.1. Dynamics of the reference impedance model

As mentioned in the introduction, one difficulty that arises in controlling an ankle prosthesis is the presence of shock forces at the heel strike. In fact, the main reason for including the series springs  $K_E$  and  $K_F$  in the mechanism (shown in Fig. 3) is to handle these impact forces. However, besides accounting for the heel strike forces in the mechanism structure, the effects of these impact forces should also be considered in the controller design. In fact, it is not enough for the controller of the prosthesis to follow a predefined initially designed trajectory for the ankle. For instance, assume the

situation where the ankle prosthesis just struck the ground at the heel of ankle prosthesis in the beginning of gait cycle. From Fig. 2 it is clear that the resultant of the impact forces at the heel ( $F_{l_1}^x$  and  $F_{l_1}^y$ ) produces a clockwise moment about the ankle that tends to intensely plantarflex it. This tendency for sudden and intense plantarflexion can weaken the performance of the prosthetic controller that is designed to smoothly adjust the angle of prosthesis and inhibit sudden plantarflexion. This prevention demands large control actions and, besides the possibility of damage to the prosthetic motor and transmission, could cause unpleasant shock forces transfer to the human body. The remedy to this problem is designing a controller to follow a reference model trajectory obtained from a reference impedance model dynamics, whose inputs are the initially designed trajectory for the ankle and the prosthesis–ground interaction moment. The idea of impedance control is to regulate both position and force by specifying a dynamic relationship between them,<sup>25,33</sup> which is appropriate for the control problems associated with human–robot interactions.<sup>34–41</sup> The reference impedance model chosen in this work is a second-order dynamics given by:

$$I_d (\ddot{\varphi}_m - \ddot{\varphi}_d) + C_d (\dot{\varphi}_m - \dot{\varphi}_d) + K_d (\varphi_m - \varphi_d) = \tau_a^{\text{ext}} \quad (11)$$

where  $I_d$ ,  $C_d$ , and  $K_d$  are the desired inertia, damping, and stiffness of the reference model, respectively.  $\varphi_d$ ,  $\dot{\varphi}_d$ , and  $\ddot{\varphi}_d$  are the initially designed trajectory, desired velocity, and the desired acceleration of ankle prosthesis, respectively. Also,  $\varphi_m$ ,  $\dot{\varphi}_m$ , and  $\ddot{\varphi}_m$  are the reference model position, velocity, and acceleration trajectories, respectively.  $\tau_a^{\text{ext}}$  is the interaction moment between the prosthesis and the ground caused by the GRFs (shown in Fig. 2).

Using positive constant values for  $I_d$ ,  $C_d$ , and  $K_d$ , the impedance model becomes stable and has two poles on the left half-plane as:

$$\begin{cases} p_1 = -\lambda' + i\lambda'' \\ p_2 = -\lambda' - i\lambda'' \end{cases} \quad (12)$$

where the parameters are such that:

$$\begin{cases} \lambda' > 0 \\ \lambda'' > 0 \\ \lambda''' \geq 0 \end{cases} \quad (13)$$

The impedance parameters  $I_d$ ,  $C_d$ , and  $K_d$  are related to the impedance pole parameters  $\lambda'$ ,  $\lambda''$ , and  $\lambda'''$  as follows:

$$\frac{d^2}{dt^2} + I_d^{-1}(C_d \frac{d}{dt} + K_d) = (\frac{d}{dt} + \lambda' - i\lambda'')(\frac{d}{dt} + \lambda' + i\lambda'') \quad (14)$$

in which  $d/dt$  is the differentiation operator.

Performance of the impedance model dynamics (11) is such that, in harmony with the value and sign of  $\tau_a^{\text{ext}}$ , the reference trajectory  $\varphi_m$  is smoothly diverged from the initially designed trajectory  $\varphi_d$ ; and when  $\tau_a^{\text{ext}}$  becomes zero, the reference model trajectory converges to the initially designed trajectory.

**Remark 1.** It is possible to choose a first-order reference impedance dynamics as:

$$C_d (\dot{\varphi}_m - \dot{\varphi}_d) + K_d (\varphi_m - \varphi_d) = \tau_a^{\text{ext}} \quad (15)$$

where the model is stable for arbitrarily selected time-varying positive damping and stiffness parameters. Compared with Eq. (11), time-varying parameters are accepted in Eq. (15), but there exist two major problems with this first-order dynamics. The first problem is that the model (Eq. 15) neglects the inertial effects of the prosthesis and therefore it is not physical. The second problem is related to the second-order nature of Euler–Lagrange equations (robot dynamics) that is not compatible with the first-order impedance dynamics (Eq. 15) to include the required impedance parameters in the designed controller as considered in this paper.

After introducing the reference impedance model, the control scheme for precisely tracking the reference impedance model trajectory  $\varphi_m$  will be presented.

### 3.2. Control algorithm

In this section, an RMRAIC scheme is presented. Note that a considerable difference between most of the robotic systems and the ankle prosthesis is the existence of physical interactions between amputee and environment. This is the main reason for employing an impedance-based controller in the present work. Before introducing the control law, the following assumption on system dynamics is expressed.

**Assumption 1.** It is reasonable to assume that the amputee intrinsically tends to control the dynamics of shank, that is, the dynamics of  $x$ ,  $y$ , and  $\theta$  is controlled naturally by the amputee (similar to an able-bodied human); however, the prosthetic controller should provide the stability and appropriately control the impedance characteristic and angular position of the ankle joint.

With the above assumption, it is only required to control the dynamics governing the ankle angle  $\varphi$ . The control signal is designed as follows:

$$\boldsymbol{\tau} = \widehat{\mathbf{D}}(\mathbf{q}) \mathbf{v}_1 + \widehat{\mathbf{C}}(\mathbf{q}, \dot{\mathbf{q}}) \mathbf{v} + \widehat{\mathbf{G}}_g(\mathbf{q}) + \mathbf{G}_e(\mathbf{q}) + \mathbf{u}_R \quad (16)$$

in which  $\mathbf{u}_R \in \mathbb{R}^4$  is the robust term of the control law given by:

$$\mathbf{u}_R = -\widehat{\gamma} \text{sgn}(\mathbf{s}) - k_1 \mathbf{s} / (\|\mathbf{s}\|^2 + k_2) \quad (17)$$

where  $k_1$  and  $k_2$  are constant positive scalars, and  $\widehat{\cdot}$  denotes the estimation of matrices, vectors, and scalars. In the control law (Eq. 16), the variables  $\mathbf{v}_1$  and  $\mathbf{v}$  are defined as:

$$\mathbf{v}_1 = \begin{Bmatrix} 0 \\ 0 \\ 0 \\ \ddot{\varphi}_d \end{Bmatrix} - I_d^{-1} \left( \begin{Bmatrix} 0 \\ 0 \\ 0 \\ C_d (\dot{\varphi} - \dot{\varphi}_d) \end{Bmatrix} + \begin{Bmatrix} 0 \\ 0 \\ 0 \\ K_d (\varphi - \varphi_d) \end{Bmatrix} - \begin{Bmatrix} 0 \\ 0 \\ 0 \\ \tau_a^{\text{ext}} \end{Bmatrix} \right) + \begin{Bmatrix} 0 \\ 0 \\ 0 \\ (\lambda''')^2 (\varphi - \varphi_m) \end{Bmatrix}$$

$$\mathbf{v} = \begin{Bmatrix} \dot{x} \\ \dot{y} \\ \dot{\theta} \\ \dot{\varphi}_m \end{Bmatrix} - \begin{Bmatrix} 0 \\ 0 \\ 0 \\ \lambda' (\varphi - \varphi_m) \end{Bmatrix} \quad (18)$$

where  $\mathbf{s} \in \mathbb{R}^4$  is the distance from sliding surface, which is given by:

$$\mathbf{s} = \dot{\mathbf{q}} - \mathbf{v} = \begin{Bmatrix} 0 \\ 0 \\ 0 \\ \dot{\varphi} - \dot{\varphi}_m + \lambda' (\varphi - \varphi_m) \end{Bmatrix} \quad (19)$$

The term  $\text{sgn}(\mathbf{s})$  in Eq. (17) is a vector whose elements are sign functions of the  $\mathbf{s}$  vector's elements. Using Property 3, the control signal  $\boldsymbol{\tau}$  (presented through Eqs. 16–19) can be expressed as:

$$\boldsymbol{\tau} = \mathbf{Y}(\mathbf{q}, \dot{\mathbf{q}}, \mathbf{v}_1, \mathbf{v}) \widehat{\boldsymbol{\theta}}_a + \mathbf{G}_e(\mathbf{q}) + \mathbf{u}_R \quad (20)$$

where  $\mathbf{Y} \widehat{\boldsymbol{\theta}}_a$  is the linear parameterization of the first three terms of the right side of Eq. (16). As mentioned before,  $\mathbf{Y}$  is the regressor matrix and  $\widehat{\boldsymbol{\theta}}_a$  is the estimation of unknown system parameters. The adaptive update law for estimation of unknown parameters is also defined as follows:

$$\dot{\widehat{\boldsymbol{\theta}}}_a = -\boldsymbol{\Gamma} \mathbf{Y}^T(\mathbf{q}, \dot{\mathbf{q}}, \mathbf{v}_1, \mathbf{v}) \mathbf{s} \quad (21)$$

where  $\boldsymbol{\Gamma} \in \mathbb{R}^{p \times p}$  is a constant symmetric and positive definite matrix. The upper bound of system uncertainties is estimated according to the following update law for the robust gain  $\widehat{\gamma}$  of the control law (Eq. 16):

$$\dot{\widehat{\gamma}} = \|\mathbf{s}\| \quad (22)$$

Finally,  $\tau_{\text{ankle}}$  (given in Eq. 2) is obtained as follows:

$$\tau_{\text{ankle}} = [0 \ 0 \ 0 \ 1] \boldsymbol{\tau} \quad (23)$$

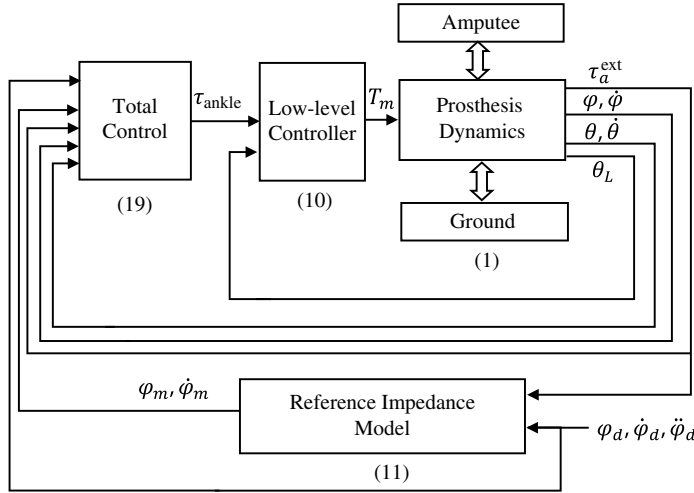


Fig. 4. The structure of the developed RMRAIC method.

Structure of the proposed controller is illustrated in Fig. 4. Regarding the developed control scheme, the only sensory information required to implement the controller is  $\theta, \varphi, \dot{\theta}, \dot{\varphi}, \theta_L$ , and  $\tau_a^{\text{ext}}$  measured from the prosthesis itself. Note that other signals  $x, y, \dot{x}$ , and  $\dot{y}$  are not required as they do not appear in the matrices and vectors of the controller (Eq. 16). Besides, it can be checked<sup>29</sup> that for the system being studied in this work, the first two columns of the matrix  $\hat{C}(\mathbf{q}, \dot{\mathbf{q}})$  are identically zero, which automatically eliminates the need for measurement of  $\dot{x}$  and  $\dot{y}$  that appear in the signal  $\mathbf{v}$  (Eq. 18).

### 3.3. Closed-loop dynamics and stability proof

The closed-loop dynamics and stability of the prosthetic system using the proposed controller are provided in Appendix A.

**Remark 2.** The designed controller is also robust against the bounded unmodeled dynamics and external disturbances, due to employing the robust control law (Eq. 17).

**Remark 3.** As shown in the proof, besides being capable of following the reference model trajectory, the designed RMRAIC controller provides the impedance characteristics of the reference impedance model (Eq. 11) for the closed-loop system as an inherent property.

## 4. Simulation Studies

In this section, performance of the developed RMRAIC scheme is evaluated using an overall amputee prosthetic foot system for the task of level ground walking.

### 4.1. Amputee model

As shown in Fig. 5, an amputee prosthetic model is simulated in the sagittal plane. In Fig. 5(a), the variables  $\varphi_1$  to  $\varphi_6$  describe the kinematic configuration of the amputee model, where  $\varphi_1$  is an absolute angle and the other angles are assumed to be relative angles. Also,  $\tau_2$  to  $\tau_6$  are joint torques acting at relative angles  $\varphi_2$  to  $\varphi_6$ , respectively. The torque  $\tau_1$ , which acts on the global angle  $\varphi_1$ , is a stabilizing moment to inhibit instability of dynamic walking motion.<sup>42</sup> Although from the bipedalism point of view the amputee model should possess one degree of under-actuation, from a biomechanical point of view, the torque  $\tau_1$  is considered as the net muscle activity existing between pelvis and trunk that inhibits instability of the amputee model. Besides, the planned trajectory for bipedal robots<sup>43</sup> is far away to be considered as a human-like trajectory, while the amputee model should be capable of generating human-like motions required by the task. The values of geometrical and inertial parameters of the amputee model (Fig. 5b) are reported in Tables I and II, respectively.

In order to simulate a level ground walking gait, the trajectories of ankle, knee, and hip are required. These trajectories are obtained from the gait experiments on human subjects.<sup>44</sup> After extracting 20-term Fourier series of position trajectories of the hip, knee, and ankle, the velocity and



Table I. Geometrical parameters of the amputee model.<sup>44</sup>

Parameter	Value
$L_1$	0.41 m
$L_2$	0.18 m
$L_3$	0.24 m
$L_4$	0.10 m
$L_5$	0.10 m
$L_6$	0.18 m
$L_7$	0.24 m
$L_8$	0.19 m
$L_9$	0.24 m

Table II. Inertial parameters of the amputee model.<sup>44</sup>

Parameter	Definition	Value
$m_T$	Trunk mass	50.85 kg
$m_t$	Thigh mass	7.50 kg
$m_s^{Amp}$	Shank mass (amputated side)	1.74 kg
$m_{s_s}$	Shank mass (sound side)	3.49 kg
$m_f$	Foot mass	1.09 kg
$I_T$	Trunk inertia	4.98 kg.m <sup>2</sup>
$I_t$	Thigh inertia	0.14 kg.m <sup>2</sup>
$I_s^{Amp}$	Shank inertia (amputated side)	0.007 kg.m <sup>2</sup>
$I_{s_s}$	Shank inertia (sound side)	0.06 kg.m <sup>2</sup>
$I_f$	Foot inertia	0.008 kg.m <sup>2</sup>

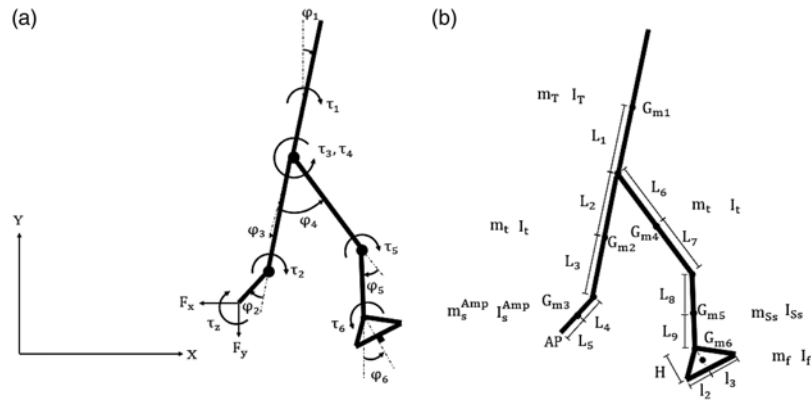


Fig. 5. Amputee model: (a) the coordinate system, kinematic variables, and positive angular directions, and (b) the geometrical and inertial parameters.

acceleration trajectories are obtained using an analytical differentiation of the corresponding Fourier series (a typical walking gait with 3 s of duration is assumed). The desired position trajectory for the trunk angle ( $\varphi_{1d}$ ) is obtained from a 20-term Fourier series of a human subject's experimental data. Also, the model and corresponding parameters of GRFs are provided in Appendix B and Table III, respectively.

After deriving the Euler–Lagrange equations of the amputee model, the ideal computed torque<sup>29</sup> is used to control the model of amputee, while the proposed controller is employed to control ankle prosthesis simultaneously.

Before presenting the simulation results, it should be noted that the “sgn” function in the control law (Eq. 17) could cause undesirable chattering in the input torque signal. Accordingly, this function

Table III. Prosthesis–ground contact model parameters.

Parameter	Value
$K_G$	$5(10^5) \frac{N}{m}$
$C_{max}$	$4(10^4) \frac{N.s}{m}$
$h$	1 mm
$h_1$	0.1
$\mu_s$	0.8
$\mu_d$	0.2
$\varepsilon_\mu$	$5 \frac{s}{m}$

Table IV. Geometrical and inertial parameters of the prosthetic system.<sup>44</sup>

Parameter	Value
$l_1$	0.24 m
$H$	0.07 m
$l_2$	0.07 m
$l_3$	0.14 m
$J_s^{com}$	0.15 m
$J_f^{com}$	0.02 m
$m_s$	1.74 kg
$I_s$	0.007 kg.m <sup>2</sup>
$m_f$	1.09 kg
$I_f$	0.008 kg.m <sup>2</sup>

Table V. Other parameter values of the prosthetic ankle mechanism used in simulations.

Parameter	Value
$K_p^r$	$0.8(10^3) \frac{N}{m}$
$R_p$	0.111 m
$r$	0.055 m
$K_E$	$6(10^5) \frac{N}{m}$
$K_F$	$3(10^5) \frac{N}{m}$
$N$	100
$\eta$	0.95

is usually replaced by approximate continuous alternatives such as saturation or tangent hyperbolic functions. In this work, the function  $sat(s/0.05)$  is used instead of the discontinuous function  $sgn(s)$  to smooth the control law in a narrow boundary layer around the sliding surface  $\mathbf{s} = \mathbf{0}$ .

#### 4.2. Simulation results

Performance of the proposed controller is evaluated using some simulation studies on an amputee prosthetic foot system in MATLAB-Simulink software. The geometrical and inertial parameters of the prosthetic system (shown in Fig. 1) are given in Table IV. Also, other parameter values of the prosthetic ankle mechanism (illustrated in Fig. 3) are reported in Table V.

The desired impedance parameters used in Eq. (11) for the appropriate physical interaction between the amputee and the ground are chosen as:  $I_d = 20 \text{ kg.m}^2$ ,  $C_d = 120 \frac{\text{kg.m}^2}{\text{s}}$ , and  $K_d = 196.2 \frac{\text{kg.m}^2}{\text{s}^2}$ . The parameters specifying the desired poles of the reference impedance model (Eq. 11) are obtained based on Eq. (14). Accordingly, these pole parameters are determined as follows:  $\lambda' = 3$ ,  $\lambda'' = 3$ ,  $\lambda''' = 0.9$ . In addition to the pole placement analysis, the stiffness parameter  $K_d$  has

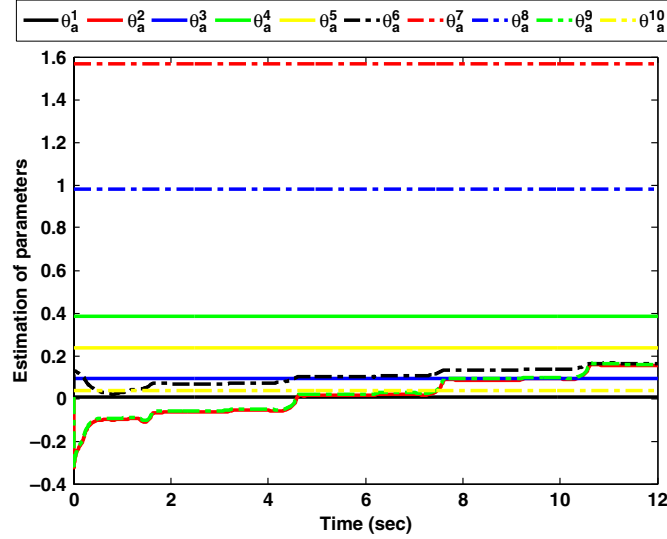


Fig. 6. Estimation of uncertain system parameters during four gait cycles using the adaptation law (21).

been chosen by a trial-and-error method such that the tracking performance of the desired ankle trajectory becomes appropriate with an error  $<0.02$  rad (as seen in Figs. 8 and 14). Moreover, too small or too large values of impedance (i.e., stiffness) parameter will negatively affect the performance of the ankle prosthesis by providing too soft or too hard haptic sense of interaction for the human operator during walking.

In this work, a prespecified walking velocity (a typical gait with 3 s of duration) is considered in simulations; however, some initial adjustment trials should be performed and analyzed to choose appropriate impedance parameters in any other motion status and/or velocity. For instance, in higher walking velocities, faster response is required to be generated by the impedance model (Eq. 11). Thus, the adjustment of poles and impedance parameters in this model should be revised in higher walking velocities.

The coefficient matrix  $\Gamma$  in the adaptation law (Eq. 21) is chosen as  $\Gamma = 50\mathbf{I}$ , where  $\mathbf{I} \in \mathbb{R}^{10 \times 10}$  is the identity matrix. The initial states of the ankle are selected equal to the corresponding states at the HS of prosthesis with the ground, and the simulation is initiated from this gait position. The initial guess of unknown system's parameter vector  $\theta_a$  is selected to have 10% error with respect to its real value. The initial value of the estimation of the uncertainties' upper bound  $\gamma$  is considered to be zero, that is,  $\hat{\gamma}(t=0) = 0$ .

The overall amputee prosthetic dynamic system is simulated during four complete gait cycles. The reason for simulating for more than one gait was to let the amputee model reach a steady-state response. Figure 6 shows the estimation of uncertain system parameters, where the parameterized vector  $\theta_a \in \mathbb{R}^{10}$  is expressed as follows:

$$\theta_a = \begin{bmatrix} m_f l_s^{\text{com}} l_f^{\text{com}}, m_f (l_f^{\text{com}})^2, m_s (l_s^{\text{com}})^2, m_s l_s^{\text{com}}, \\ m_f l_s^{\text{com}}, m_f l_f^{\text{com}}, m_s, m_f, I_f, I_s \end{bmatrix}^T \quad (24)$$

As seen in Fig. 6, the estimations have remained bounded during the entire time of gait cycles. Figure 7 demonstrates the estimation of the upper bound of system's uncertainties during four gait cycles. Note that these estimations are made constant inside a chosen narrow boundary layer around the sliding surface  $\mathbf{s} = \mathbf{0}$ , as described by Slotine and Coetsee in ref. [45].

The differences between the impedance model position trajectory and the desired position trajectory, and the tracking error in one gait cycle are illustrated in Fig. 8. Note that the tracking error is significantly small and acceptable, although the control law is smoothed inside a narrow boundary layer around the sliding surface  $\mathbf{s} = \mathbf{0}$  to avoid chattering. The plot of translational and angular positions of the amputated place is given in Fig. 9. Also, the plot of  $\varphi - \dot{\varphi}$  during four complete gait cycles is given in Fig. 10. As seen, the position trajectory converged to a limit cycle.

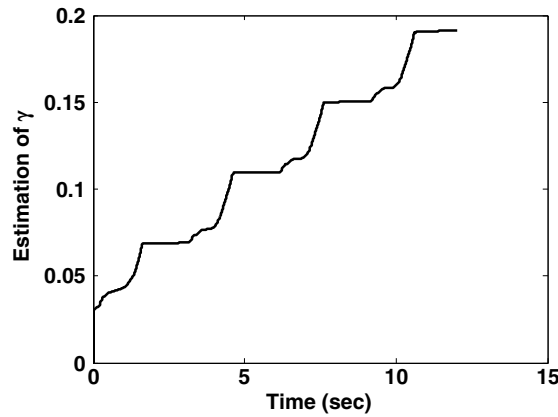


Fig. 7. Estimation of the upper bound of system's uncertainties by the update rule (22).

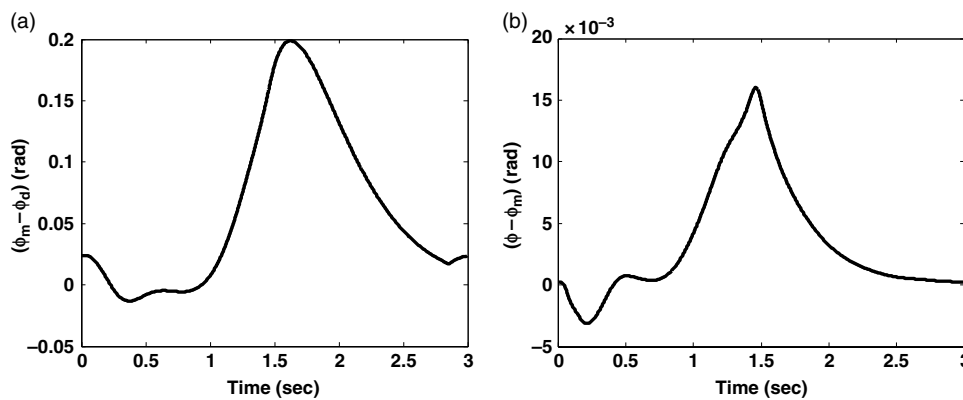


Fig. 8. (a) Difference between the reference model response and the initially designed trajectory, and (b) the tracking error in one gait cycle.

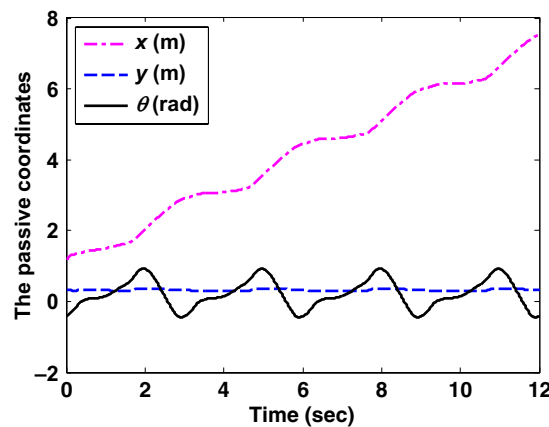


Fig. 9. Translational and angular positions of the amputated place during four complete gait cycles.

The control signal  $\tau_{ankle}$  for one gait cycle is shown in Fig. 11. As observed in this figure, there exists a jump in  $\tau_{ankle}$  during a gait cycle. This jump is due to the HS of prosthesis with the ground at the beginning of each gait cycle as discussed previously. Finally, the motor torque  $T_m$  and the torques  $T_m^{NSE}$  and  $T^{SSE}$  (illustrating the effects of the mechanism's spring) are presented in Fig. 12. It should be mentioned that the computation of  $T_{SSE}$  requires angle  $\theta_L$ . Since  $\theta_L$  was not available in the computation, an assumption was utilized that the interaction moment between ground and prosthesis about the ankle joint is approximately equal to the moment produced by the compression springs of SEA mechanism about the ankle joint at each instance of the stance phase. Using this assumption,

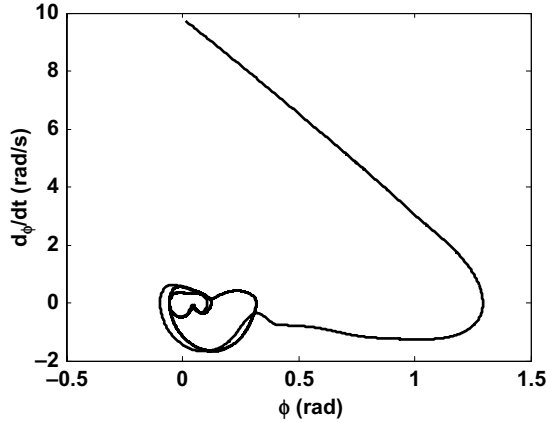


Fig. 10. Trajectory of  $\phi - \dot{\phi}$  converging to a limit cycle during four complete gait cycles.

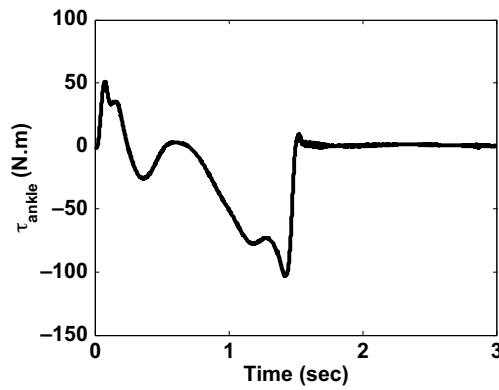


Fig. 11. Input torque  $\tau_{ankle}$  applied at the ankle joint of the prosthesis during one gait cycle.

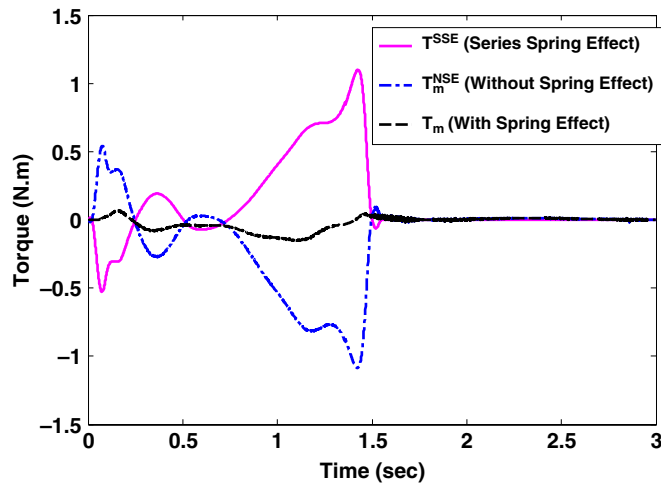


Fig. 12. Motor torque in the presence of spring effect  $T_m$ , spring effect  $T^{SSE}$ , and motor torque in the absence of spring effect  $T_m^{NSE}$  during one gait cycle.

an approximation for  $\theta_L$  is obtained. Figure 12 shows how prosperous is the SEA mechanism in reducing the impact at the heel strike (which is better seen in Fig. 11). In Fig. 12,  $T_m$  stands for the motor torque when the SEA mechanism is used, and  $T_m^{NSE}$  is the corresponding torque in the absence of any series spring. Figure 12 also shows how the effect of series spring torque ( $T^{SSE}$ ) has reduced the required torque by the motor from  $T_m^{NSE}$  to  $T_m$ , and prevented HS impact and shock loads.

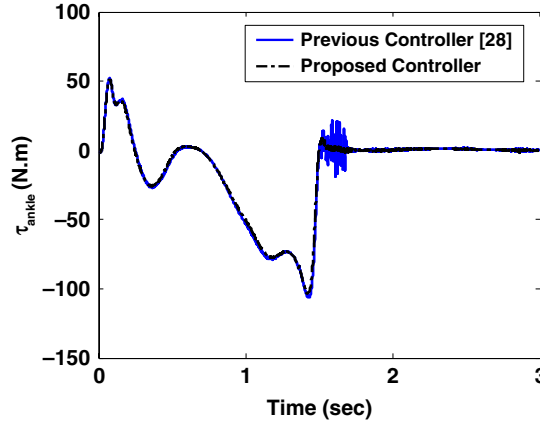


Fig. 13. Comparison between input torque  $\tau_{\text{ankle}}$  and torque produced using the previous control method developed in ref. [28].

To better investigate the performance of the developed control scheme, a comparison with a recently developed control method<sup>28</sup> for an active prosthesis is carried out in this section. Assuming similar parameters and gains, the control law in ref. [28] is expressed as follows:

$$\boldsymbol{\tau} = \mathbf{Y}(\mathbf{q}, \dot{\mathbf{q}}, \mathbf{v}_A, \dot{\mathbf{v}}_A) \hat{\boldsymbol{\theta}}_a + \mathbf{G}_c(\mathbf{q}) - \mathbf{J}^T \mathbf{F}_e - \Gamma_D^A \text{sat}(\mathbf{s}_A / \text{diag}(\varphi_A)) \quad (25)$$

where  $\mathbf{e}$ ,  $\mathbf{v}_A$ ,  $\mathbf{s}_A$  are given as

$$\begin{cases} \mathbf{e} = \mathbf{q} - \mathbf{q}_m \\ \mathbf{s}_A = \dot{\mathbf{e}} + \lambda_A \mathbf{e} \\ \mathbf{v}_A = \dot{\mathbf{q}}_m - \lambda_A \mathbf{e} \end{cases} \quad (26)$$

Moreover, the estimation of parameters is updated based on the dynamics:

$$\hat{\boldsymbol{\theta}}_a = -\Gamma_A \mathbf{Y}^T(\mathbf{q}, \dot{\mathbf{q}}, \mathbf{v}, \dot{\mathbf{v}}) \mathbf{s}_\Delta \quad (27)$$

where  $\mathbf{s}_\Delta$  is given by:

$$\mathbf{s}_\Delta = \mathbf{s}_A - \varphi_A \text{sat}(\mathbf{s}_A / \text{diag}(\varphi_A)) \quad (28)$$

The control parameters  $\Gamma_D^A = 20$ ,  $\varphi_A = 0.1$ ,  $\lambda_A = 3$ ,  $\Gamma_A = 0.01$  are used in the simulation. Also, the position and velocity trajectories  $\mathbf{q}_m$  and  $\dot{\mathbf{q}}_m$  can be obtained from the reference impedance dynamics:

$$I_A (\ddot{\mathbf{q}}_m - \ddot{\mathbf{q}}_d) + C_A (\dot{\mathbf{q}}_m - \dot{\mathbf{q}}_d) + K_A (\mathbf{q}_m - \mathbf{q}_d) = \mathbf{J}^T \mathbf{F}_e \quad (29)$$

where the impedance parameters are  $I_A = 20$ ,  $C_A = 120$ ,  $K_A = 196.2$ . The previous control method<sup>28</sup> defined in Eqs. (25–29) is similar to the controller (Eq. 16) developed in this paper except for two distinctions. As the first one, the previous controller<sup>28</sup> was designed for the ankle joint and the amputated place simultaneously. Therefore, the feedback of  $x$ ,  $y$ ,  $\dot{x}$ ,  $\dot{y}$  is required to implement the control law in ref. [28], which is difficult to be measured and unnecessary for the control as discussed in Section 3.2. The second distinction of the previous controller<sup>28</sup> in comparison with the proposed RMRAIC strategy is the isolation of the control law and the reference impedance model (Eq. 29), which results in a lack of inclusion of impedance parameters in the control scheme as provided in this paper. Note that, though the feedback of GRFs is required to implement in the control law,<sup>28</sup> it is not a shortcoming of this controller since the estimation of GRFs is currently under investigation by the same researchers.<sup>46</sup> Figure 13 shows a comparison of ankle torques obtained by the proposed and previous control strategies during one gait cycle. As seen, the responses are coincident except for the late stance phase, which is due to a lack of impedance inclusion in the control law developed in ref. [28]. The differences between the reference model response trajectory and the initially designed trajectory, and comparison of the tracking errors during four complete gait cycles are given for the proposed and previous control strategies in Fig. 14. Two time-series in Fig. 14(a) are coincident for

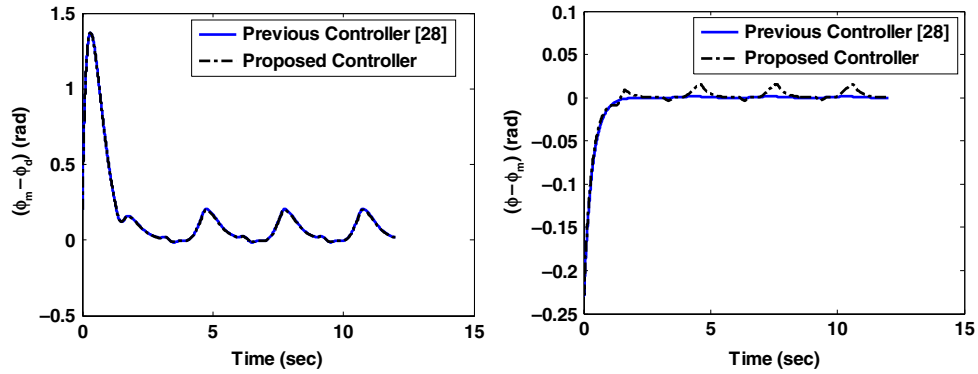


Fig. 14. Comparison of responses obtained from the proposed and previous<sup>28</sup> control strategies: (a) differences between the reference model response and the initially designed trajectory, and (b) tracking errors during four complete gait cycles.

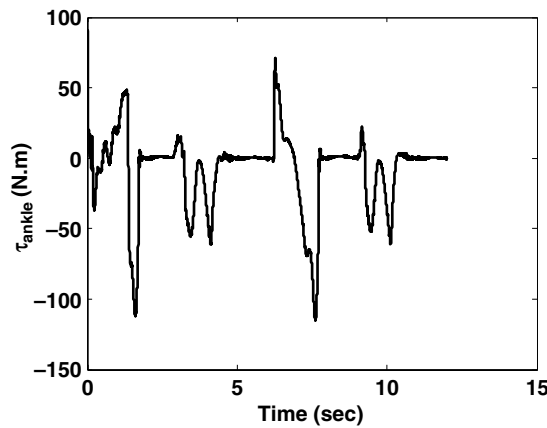


Fig. 15. Input torque  $\tau_{\text{ankle}}$  during four gait cycles of walking on a surface specified with  $Y = 0.04 \sin(2X)$ .

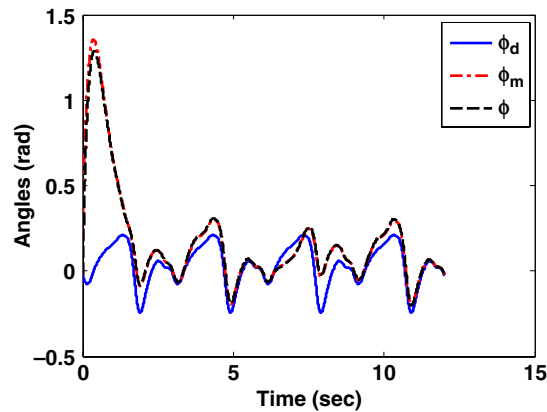


Fig. 16. Initially designed ( $\phi_d$ ), impedance ( $\phi_m$ ), and ankle ( $\phi$ ) trajectories during four complete gait cycles of walking on an uneven surface specified with  $Y = 0.04 \sin(2X)$ .

both controllers, which was expected due to the same reference impedance dynamics. Figure 14(b) shows that the tracking error of the previous method<sup>28</sup> is better than the one obtained by the method developed in this paper. This can be justified since the effects of GRFs are included in ref. [28], while this is not the case for the currently proposed method. In fact, the GRFs are assumed not to be measurable in this paper; and due to the absence of their effects in the control design, the tracking performance is worse than the one obtained in ref. [28].

To better show the effectiveness of the proposed strategy, the performance of this control scheme in an uneven ground is investigated. Figure 15 shows the control input during walking on a ground surface specified with the relation:

$$Y = 0.04 \sin(2X) \quad (30)$$

The desired, impedance, and ankle trajectories for this task are provided in Fig. 16, and the performance of the control scheme is justified.

## 5. Conclusion

An asymptotically stable RMRAIC scheme was presented in this work for active ankle prostheses. The controller was designed to track the output trajectory of a second-order impedance dynamics whose inputs are the initially designed trajectory for the ankle joint and the prosthesis–ground interaction moment. It was analytically proven and also shown via numerical simulations that the controller was robust against parametric uncertainties and disturbances. The SEA mechanism was employed in the design of prosthetic structure. The results showed the prosperity of the proposed prosthetic mechanism in filtering the shock forces exerted to the system (e.g., due to HS) and also the success of the designed mechanism in reducing the required torque generated by the motor. It should be highlighted that more experimental evaluations of the proposed control strategy for active prostheses will be conducted in future works. Moreover, the proposed control strategy can be used for other tasks and/or other prosthetic systems.

## References

1. J. J. Rice, J. M. Schimmels and S. Huang, "Design and evaluation of a passive ankle prosthesis with powered push-off," *J. Mech. Rob.* **8**, 021012 (2016).
2. S. H. Collins and A. D. Kuo, "Recycling energy to restore impaired ankle function during human walking," *PLoS one* **5**, e9307 (2010).
3. H. Bateni and S. J. Olney, "Kinematic and kinetic variations of below-knee amputee gait," *JPO* **14**, 2–10 (2002).
4. G. R. Colborne, S. Naumann, P. E. Longmuir and D. Berbrayer, "Analysis of mechanical and metabolic factors in the gait of congenital below knee amputees: A comparison of the SACH and Seattle feet," *Am. J. Phys. Med. Rehabil.* **71**, 272–278 (1992).
5. N. Molen, "Energy/speed relation of below-knee amputees walking on a motor-driven treadmill," *Eur. J. Appl. Physiol. Occup. Physiol.* **31**, 173–185 (1973).
6. S. K.-W. Au, Powered ankle-foot prosthesis for the improvement of amputee walking economy. *Ph.D. Dissertation* (Massachusetts Institute of Technology, 2007).
7. R. D. Bellman, M. A. Holgate and T. G. Sugar, "SPARKy 3: Design of an active robotic ankle prosthesis with two actuated degrees of freedom using regenerative kinetics," *2nd IEEE RAS & EMBS International Conference on Biomedical Robotics and Biomechatronics*, Scottsdale, AZ, USA (2008) pp. 511–516.
8. F. Sup, A. Bohara and M. Goldfarb, "Design and control of a powered transfemoral prosthesis," *Int. J. Rob. Res.* **27**, 263–273 (2008).
9. R. Suzuki, T. Sawada, N. Kobayashi and E. P. Hofer, "Control method for powered ankle prosthesis via internal model control design," *2011 International Conference on Mechatronics and Automation (ICMA)*, IEEE, Beijing, China (2011) pp. 237–242.
10. R. Versluys, A. Desomer, G. Lenaerts, M. Van Damme, P. Beyl, G. Van der Perre, L. Peeraer and D. Lefeber, "A pneumatically powered below-knee prosthesis: Design specifications and first experiments with an amputee," *2nd IEEE RAS & EMBS International Conference on Biomedical Robotics and Biomechatronics, 2008, BioRob 2008*, IEEE, Scottsdale, AZ, USA (2008) pp. 372–377.
11. J. K. Hitt, R. Bellman, M. Holgate, T. G. Sugar and K. W. Hollander, "The sparky (spring ankle with regenerative kinetics) project: Design and analysis of a robotic transtibial prosthesis with regenerative kinetics," *ASME International Design Engineering Technical Conferences and Computers and Information in Engineering Conference*, Las Vegas, NV, USA (2007) pp. 1587–1596.
12. S. K. Au, J. Weber and H. Herr, "Biomechanical design of a powered ankle-foot prosthesis," *IEEE 10th International Conference on Rehabilitation Robotics*, Noordwijk, Netherlands (2007) pp. 298–303.
13. J. M. Caputo and S. H. Collins, "A universal ankle-foot prosthesis emulator for human locomotion experiments," *J. Biomech. Eng.* **136**, 035002 (2014).
14. D. H. Gates, *Characterizing Ankle Function During Stair Ascent, Descent, and Level Walking for Ankle Prosthesis and Orthosis Design* (University of Boston, 2004).
15. M. L. Palmer, *Sagittal Plane Characterization of Normal Human Ankle Function Across a Range of Walking Gait Speeds* (MIT, 2002).
16. G. Klute, J. Czerniecki and B. Hannaford, "Development of powered prosthetic lower limb," *Proceedings of the 1st National Meeting, Veterans Affairs Rehabilitation Research and Development Service*, Washington, DC, USA (1998).



17. S. K. Au, J. Weber and H. Herr, "Powered Ankle-Foot Prosthesis Improves Walking Metabolic Economy," *IEEE Trans. Rob.* **25**, 51–66 (2009).
18. D. W. Robinson, *Design and Analysis of Series Elasticity in Closed-loop Actuator Force Control* (Massachusetts Institute of Technology, 2000).
19. M. M. Williamson, Series Elastic Actuators, A. I. Technical Report, No. 1524 (1995).
20. M. A. Holgate, T. G. Sugar and A. W. Bohler, "A novel control algorithm for wearable robotics using phase plane invariants," *IEEE International Conference on Robotics and Automation, ICRA'09*, Kobe, Japan (2009) pp. 3845–3850.
21. K. W. Hollander, R. Ilg, T. G. Sugar and D. Herring, "An efficient robotic tendon for gait assistance," *J. Biomech. Eng.* **128**, 788–791 (2006).
22. K. Yuan, J. Zhu, Q. Wang and L. Wang, "Finite-state control of powered below-knee prosthesis with ankle and toe," *IFAC Proc.* **44**, 2865–2870 (2011).
23. J. Zhu, Q. Wang and L. Wang, "PANTOE 1: Biomechanical design of powered ankle-foot prosthesis with compliant joints and segmented foot," *2010 IEEE/ASME International Conference on Advanced Intelligent Mechatronics*, Montreal, ON, Canada (2010) pp. 31–36.
24. G. A. Pratt and M. M. Williamson, "Series elastic actuators," *Intelligent Robots and Systems 95: Human Robot Interaction and Cooperative Robots*, *IEEE/RSJ International Conference on Proceedings*, Pittsburgh, PA, USA, vol. 1 (1995) pp. 399–406.
25. N. Hogan, "Impedance control: An approach to manipulation," *J. Dyn. Syst. Meas. Control* **107**, 17 (1985).
26. J. A. Blaya and H. Herr, "Adaptive control of a variable-impedance ankle-foot orthosis to assist drop-foot gait," *IEEE Trans. Neural Syst. Rehabil. Eng.* **12**, 24–31 (2004).
27. A. Mai and S. Commuri, "Intelligent control of a prosthetic ankle joint using gait recognition," *Control Eng. Pract.* **49**, 1–13 (2016).
28. V. Azimi, S. A. Fakoorian, T. T. Nguyen and D. Simon, "Robust adaptive impedance control with application to a transfemoral prosthesis and test robot," *J. Dyn. Syst. Meas. Control* **140**, 121002 (2018).
29. J.-J. E. Slotine and W. Li, *Applied Nonlinear Control* (Prentice-Hall, Englewood Cliffs, NJ, 1991).
30. M. W. Spong, S. Hutchinson and M. Vidyasagar, *Robot Modeling and Control* (Wiley, New York, 2006).
31. M. Sadedel, A. Yousefi-Koma, M. Khadiv and S. Mansouri, "Investigation on dynamic modeling of SURENA III humanoid robot with heel-off and heel-strike motions," *Iran. J. Sci. Technol. Trans. Mech. Eng.* **41**, 9–23 (2017).
32. F. Hashemzadeh and M. Tavakoli, "Position and force tracking in nonlinear teleoperation systems under varying delays," *Robotica* **33**, 1003–1016 (2015).
33. T. Zhang, L. Jiang, S. Fan, X. Wu and W. Feng, "Development and experimental evaluation of multi-fingered robot hand with adaptive impedance control for unknown environment grasping," *Robotica* **34**, 1168–1185 (2016).
34. V. Azimi, D. Simon and H. Richter, "Stable robust adaptive impedance control of a prosthetic leg," *American Society of Mechanical Engineers Dynamic Systems and Control Conference*, ASME 2015, Columbus, Ohio, USA (2015) pp. V001T009A003–V001T009A003.
35. M. Sharifi, S. Behzadipour and H. Salarieh, "Nonlinear bilateral adaptive impedance control with applications in telesurgery and telerehabilitation," *J. Dyn. Syst. Meas. Control* **138**, 111010 (2016).
36. V. Azimi, T. Shu, H. Zhao, E. Ambrose, A. D. Ames and D. Simon, "Robust control of a powered transfemoral prosthesis device with experimental verification," *American Control Conference (ACC), 2017*, IEEE, Seattle, WA, USA (2017) pp. 517–522.
37. V. Azimi, D. Simon, H. Richter and S. A. Fakoorian, "Robust composite adaptive transfemoral prosthesis control with non-scalar boundary layer trajectories," *American Control Conference (ACC), 2016*, IEEE (2016) pp. 3002–3007.
38. M. Sharifi, S. Behzadipour, H. Salarieh and M. Tavakoli, "Cooperative modalities in robotic tele-rehabilitation using nonlinear bilateral impedance control," *Control Eng. Pract.* **67**, 52–63 (2017).
39. M. Sharifi, S. Behzadipour and G. Vossoughi, "Model reference adaptive impedance control of rehabilitation robots in operational space," *4th IEEE RAS & EMBS International Conference on Biomedical Robotics and Biomechatronics (BioRob)*, IEEE, Rome, Italy (2012) pp. 1698–1703.
40. M. Sharifi, H. Salarieh, S. Behzadipour and M. Tavakoli, "Tele-echography of moving organs using an impedance-controlled telerobotic system," *Mechatronics* **45**, 60–70 (2017).
41. M. Najafi, M. Sharifi, K. Adams and M. Tavakoli, "Robotic assistance for children with cerebral palsy based on learning from tele-cooperative demonstration," *Int. J. Intell. Rob. Appl.* **1**, 43–54 (2017).
42. M. Wojtyra, "Multibody simulation model of human walking," *Mech. Based Des. Struct. Mach. Int. J.* **31**(3), 357–377 (2003).
43. E. R. Westervelt, J. W. Grizzle, C. Chevallereau, J. H. Choi and B. Morris, *Feedback Control of Dynamic Bipedal Robot Locomotion* (CRC Press, Boca Raton, 2007).
44. D. A. Winter, *Biomechanics and Motor Control of Human Movement* (John Wiley & Sons, New York, 2009).
45. J.-J. Slotine and J. Coetsee, "Adaptive sliding controller synthesis for non-linear systems," *Int. J. Control* **43**, 1631–1651 (1986).
46. V. Azimi, T. T. Nguyen, M. Sharifi, S. A. Fakoorian and D. Simon, "Robust ground reaction force estimation and control of lower-limb prostheses: Theory and simulation," *IEEE Trans. Syst. Man Cybern. Syst.* **99**, 1–12 (2018).

47. K. S. Narendra and A. M. Annaswamy, *Stable Adaptive Systems* (Prentice-Hall, New Jersey, 2012).  
 48. M. Peasgood, E. Kubica and J. McPhee, "Stabilization of a dynamic walking gait simulation," *J Comput. Nonlinear Dyn.* **2**, 65–72 (2007).

### Appendix A: Closed-loop dynamics and stability proof

The proposed control objective is that the developed RMRAIC method makes the closed-loop dynamics of the ankle prosthesis similar to the reference impedance model (Eq. 11), and the ankle trajectory asymptotically tracks the response of Eq. (11).

The closed-loop dynamics of the system using the proposed RMRAIC controller should be obtained for stability analysis. For this purpose, the control law (Eq. 16) is substituted into the system dynamics (Eq. 1):

$$\mathbf{D}(\mathbf{q}) \ddot{\mathbf{q}} + \mathbf{C}(\mathbf{q}, \dot{\mathbf{q}}) \dot{\mathbf{q}} + \tilde{\mathbf{G}}_g(\mathbf{q}) = \widehat{\mathbf{D}}(\mathbf{q}) \mathbf{v}_1 + \widehat{\mathbf{C}}(\mathbf{q}, \dot{\mathbf{q}}) \mathbf{v} + \widehat{\mathbf{G}}_g(\mathbf{q}) + \mathbf{u}_R + \mathbf{J}^T \mathbf{F}_e \quad (\text{A1})$$

Subtracting  $\mathbf{D}(\mathbf{q}) \mathbf{v}_1 + \mathbf{C}(\mathbf{q}, \dot{\mathbf{q}}) \mathbf{v} + \mathbf{G}_g(\mathbf{q})$  from both sides of Eq. (A1) results in:

$$\mathbf{D}(\mathbf{q}) (\ddot{\mathbf{q}} - \mathbf{v}_1) + \mathbf{C}(\mathbf{q}, \dot{\mathbf{q}}) (\dot{\mathbf{q}} - \mathbf{v}) = \tilde{\mathbf{D}}(\mathbf{q}) \mathbf{v}_1 + \tilde{\mathbf{C}}(\mathbf{q}, \dot{\mathbf{q}}) \mathbf{v} + \tilde{\mathbf{G}}_g(\mathbf{q}) + \mathbf{u}_R + \mathbf{J}^T \mathbf{F}_e \quad (\text{A2})$$

where  $\tilde{\mathbf{D}}(\mathbf{q})$ ,  $\tilde{\mathbf{C}}(\mathbf{q}, \dot{\mathbf{q}})$  and  $\tilde{\mathbf{G}}_g(\mathbf{q})$  are the estimation errors of the dynamic matrices  $\mathbf{D}(\mathbf{q})$ ,  $\mathbf{C}(\mathbf{q}, \dot{\mathbf{q}})$  and  $\mathbf{G}_g(\mathbf{q})$ , respectively, defined as:

$$\begin{aligned} \tilde{\mathbf{D}}(\mathbf{q}) &= \widehat{\mathbf{D}}(\mathbf{q}) - \mathbf{D}(\mathbf{q}) \\ \tilde{\mathbf{C}}(\mathbf{q}, \dot{\mathbf{q}}) &= \widehat{\mathbf{C}}(\mathbf{q}, \dot{\mathbf{q}}) - \mathbf{C}(\mathbf{q}, \dot{\mathbf{q}}) \\ \tilde{\mathbf{G}}_g(\mathbf{q}) &= \widehat{\mathbf{G}}_g(\mathbf{q}) - \mathbf{G}_g(\mathbf{q}) \end{aligned}$$

As a consequence of Property 3 in Section 2.1, one can write:

$$\tilde{\mathbf{D}}(\mathbf{q}) \mathbf{v}_1 + \tilde{\mathbf{C}}(\mathbf{q}, \dot{\mathbf{q}}) \mathbf{v} + \tilde{\mathbf{G}}_g(\mathbf{q}) = \mathbf{Y}(\mathbf{q}, \dot{\mathbf{q}}, \mathbf{v}_1, \mathbf{v}) (\widehat{\boldsymbol{\theta}}_a - \boldsymbol{\theta}_a) \quad (\text{A3})$$

Therefore, Eq. (A2) is simplified to:

$$\mathbf{D}(\mathbf{q}) (\ddot{\mathbf{q}} - \mathbf{v}_1) + \mathbf{C}(\mathbf{q}, \dot{\mathbf{q}}) (\dot{\mathbf{q}} - \mathbf{v}) = \mathbf{Y}(\mathbf{q}, \dot{\mathbf{q}}, \mathbf{v}_1, \mathbf{v}) \tilde{\boldsymbol{\theta}}_a + \mathbf{u}_R + \mathbf{J}^T \mathbf{F}_e \quad (\text{A4})$$

in which  $\tilde{\boldsymbol{\theta}}_a$  is the parameter estimation error vector defined as

$$\tilde{\boldsymbol{\theta}}_a = \widehat{\boldsymbol{\theta}}_a - \boldsymbol{\theta}_a \quad (\text{A5})$$

The vector  $\ddot{\mathbf{q}} - \mathbf{v}_1$  appearing in Eq. (A4) can be written as

$$\ddot{\mathbf{q}} - \mathbf{v}_1 = \mathbf{v}_2 - \mathbf{v}_2^p \quad (\text{A6})$$

where the auxiliary signal  $\mathbf{v}_2 \in \mathbb{R}^4$  is obtained as follows:

$$\mathbf{v}_2 = \left\{ \begin{array}{c} 0 \\ 0 \\ 0 \\ \ddot{\varphi} - \ddot{\varphi}_d + I_d^{-1} (C_d (\dot{\varphi} - \dot{\varphi}_d) + K_d (\varphi - \varphi_d) - \tau_a^{ext}) - (\lambda''')^2 (\varphi - \varphi_m) \end{array} \right\} \quad (\text{A7})$$

Also,  $\mathbf{v}_2^p \in \mathbb{R}^4$  in Eq. (A6) is a bounded perturbation-like term given by:

$$\mathbf{v}_2^p = \left\{ \begin{array}{c} -\ddot{x} \\ -\ddot{y} \\ -\ddot{\theta} \\ 0 \end{array} \right\} \quad (\text{A8})$$

Using Eq. (A6) and according to Eq. (19) ( $\dot{\mathbf{q}} - \mathbf{v} = \mathbf{s}$ ), Eq. (A4) can be simplified to:

$$\mathbf{D}(\mathbf{q}) \mathbf{v}_2 + \mathbf{C}(\mathbf{q}, \dot{\mathbf{q}}) \mathbf{s} = \mathbf{Y}(\mathbf{q}, \dot{\mathbf{q}}, \mathbf{v}_1, \mathbf{v}) \tilde{\boldsymbol{\theta}}_a + \mathbf{u}_R + \mathbf{J}^T \mathbf{F}_e + \mathbf{D}(\mathbf{q}) \mathbf{v}_2^p \quad (\text{A9})$$

The reference impedance model dynamics (Eq. 11) can be written in a vector notation as

$$\mathbf{v}_3 = \mathbf{0} \quad (\text{A10})$$

where  $\mathbf{v}_3 \in \mathbb{R}^4$  is an auxiliary signal expressed as

$$\mathbf{v}_3 = \left\{ \begin{array}{c} 0 \\ 0 \\ 0 \\ \ddot{\varphi}_m - \ddot{\varphi}_d + I_d^{-1} (C_d (\dot{\varphi}_m - \dot{\varphi}_d) + K_d (\varphi_m - \varphi_d) - \tau_a^{ext}) \end{array} \right\} \quad (\text{A11})$$

Based on Property 1, the matrix  $\mathbf{D}$  is positive definite and invertible. Invertibility of  $\mathbf{D}$  implies that the only solution to the following equation:

$$\mathbf{D}(\mathbf{q}) \mathbf{v}_3 = \mathbf{0} \quad (\text{A12})$$

is the trivial solution given by Eq. (A10). Therefore, Eqs. (A10) and (A12) are equivalent and can be used interchangeably. Subtracting  $\mathbf{D}(\mathbf{q}) \mathbf{v}_3$  from the left-hand side of Eq. (A9) leads to:

$$\mathbf{D}(\mathbf{q}) \mathbf{v}_4 + \mathbf{C}(\mathbf{q}, \dot{\mathbf{q}}) \mathbf{s} = \mathbf{Y}(\mathbf{q}, \dot{\mathbf{q}}, \mathbf{v}_1, \mathbf{v}) \tilde{\boldsymbol{\theta}}_a + \mathbf{u}_R + \mathbf{J}^T \mathbf{F}_e + \mathbf{D}(\mathbf{q}) \mathbf{v}_2^p \quad (\text{A13})$$

where the signal  $\mathbf{v}_4 \in \mathbb{R}^4$  is obtained as:

$$\mathbf{v}_4 = \mathbf{v}_2 - \mathbf{v}_3 = \left\{ \begin{array}{c} 0 \\ 0 \\ 0 \\ \ddot{\varphi} - \ddot{\varphi}_m + I_d^{-1} (C_d (\dot{\varphi} - \dot{\varphi}_m) + K_d (\varphi - \varphi_m)) - (\lambda''')^2 (\varphi - \varphi_m) \end{array} \right\} \quad (\text{A14})$$

By applying both sides of the operator relation (Eq. 14) to the signal  $\varphi - \varphi_m$  and employing Eq. (19), it can be concluded after some mathematical manipulations that:

$$\mathbf{v}_4 = \dot{\mathbf{s}} + \lambda'' \mathbf{s} \quad (\text{A15})$$

Therefore, the closed-loop error dynamics (Eq. A13) can be simplified as

$$\mathbf{D}(\mathbf{q}) (\dot{\mathbf{s}} + \lambda'' \mathbf{s}) + \mathbf{C}(\mathbf{q}, \dot{\mathbf{q}}) \mathbf{s} = \mathbf{Y}(\mathbf{q}, \dot{\mathbf{q}}, \mathbf{v}_1, \mathbf{v}) \tilde{\boldsymbol{\theta}}_a + \mathbf{u}_R + \mathbf{J}^T \mathbf{F}_e + \mathbf{D}(\mathbf{q}) \mathbf{v}_2^p \quad (\text{A16})$$

Equation (A16) expresses the closed-loop dynamics of controlled prosthesis. Before presenting the Lyapunov stability analysis, the last two terms on the right-hand side of Eq. (A16) are discussed. Since the elements of  $\mathbf{D}$  and  $\mathbf{J}$  matrices only comprised sine and cosine functions of  $\theta$ ,  $\varphi$ , and the signals  $\mathbf{v}_2^p$  (given in Eq. A8) and  $\mathbf{F}_e$  consisted of bounded elements, the following inequality can be presented:

$$\|\mathbf{J}^T \mathbf{F}_e + \mathbf{D}(\mathbf{q}) \mathbf{v}_2^p\| \leq \gamma \quad (\text{A17})$$

where  $\gamma$  is assumed to be an unknown and constant positive scalar and  $\|\cdot\|$  is used for the Euclidean norm of vectors. To prove system stability and the asymptotic tracking performance, the following Lyapunov function candidate is employed:

$$V(\mathbf{s}, \tilde{\boldsymbol{\theta}}_a, \tilde{\gamma}) = \frac{1}{2} \mathbf{s}^T \mathbf{D}(\mathbf{q}) \mathbf{s} + \frac{1}{2} \tilde{\boldsymbol{\theta}}_a^T \boldsymbol{\Gamma}^{-1} \tilde{\boldsymbol{\theta}}_a + \frac{1}{2} \tilde{\gamma}^2 \quad (\text{A18})$$

where  $\tilde{\gamma}$  is the estimation error of  $\gamma$  ( $\tilde{\gamma} = \hat{\gamma} - \gamma$ ). Using the closed-loop dynamics (Eq. A16), and noticing that the vector of unknown parameters  $\boldsymbol{\theta}_a$  and the upper bound  $\gamma$  have constant values, the time derivative of  $V$  can be expressed as:

$$\begin{aligned} \dot{V} &= \mathbf{s}^T (-\lambda'' \mathbf{D}(\mathbf{q}) \mathbf{s} - \mathbf{C}(\mathbf{q}, \dot{\mathbf{q}}) \mathbf{s} + \mathbf{Y}(\mathbf{q}, \dot{\mathbf{q}}, \mathbf{v}_1, \mathbf{v}) \tilde{\boldsymbol{\theta}}_a + \mathbf{u}_R + \mathbf{J}^T \mathbf{F}_e + \mathbf{D}(\mathbf{q}) \mathbf{v}_2^p) \\ &\quad + \frac{1}{2} \mathbf{s}^T \dot{\mathbf{D}}(\mathbf{q}) \mathbf{s} + \tilde{\boldsymbol{\theta}}_a^T \boldsymbol{\Gamma}^{-1} \dot{\tilde{\boldsymbol{\theta}}}_a + \tilde{\gamma} \dot{\tilde{\gamma}} \end{aligned} \quad (\text{A19})$$

Substituting the update law (Eq. 21) for the estimated parameters  $\hat{\boldsymbol{\theta}}_a$ , and arranging and simplifying the terms in Eq. (A19), we get:

$$\dot{V} = -\lambda'' \mathbf{s}^T \mathbf{D}(\mathbf{q}) \mathbf{s} + \mathbf{s}^T \mathbf{u}_R + \mathbf{s}^T (\mathbf{J}^T \mathbf{F}_e + \mathbf{D}(\mathbf{q}) \mathbf{v}_2^p) + \frac{1}{2} \mathbf{s}^T (\dot{\mathbf{D}}(\mathbf{q}) - 2\mathbf{C}(\mathbf{q}, \dot{\mathbf{q}})) \mathbf{s} + \tilde{\gamma} \dot{\tilde{\gamma}} \quad (\text{A20})$$

Due to Property 2, and since the quadratic term associated with a skew symmetric matrix  $(\dot{\mathbf{D}}-2\mathbf{C})$  is identically zero, the time derivative of Lyapunov function is simplified to:

$$\dot{V} = -\lambda'' \mathbf{s}^T \mathbf{D}(\mathbf{q}) \mathbf{s} + \mathbf{s}^T \mathbf{u}_R + \mathbf{s}^T (\mathbf{J}^T \mathbf{F}_e + \mathbf{D}(\mathbf{q}) \mathbf{v}_2^p) + \tilde{\gamma} \hat{\gamma} \quad (\text{A21})$$

Based on Eq. (A17), the following inequality can be written:

$$\mathbf{s}^T (\mathbf{J}^T \mathbf{F}_e + \mathbf{D}(\mathbf{q}) \mathbf{v}_2^p) \leq \|\mathbf{s}\| \|\mathbf{J}^T \mathbf{F}_e + \mathbf{D}(\mathbf{q}) \mathbf{v}_2^p\| \leq \|\mathbf{s}\| \gamma \quad (\text{A22})$$

In addition, using Eq. (17) the term  $\mathbf{s}^T \mathbf{u}_R$  in Eq. (A21) can be expressed as

$$\mathbf{s}^T \mathbf{u}_R = -\hat{\gamma} (|s_1| + |s_2| + |s_3| + |s_4|) - k_1 \|\mathbf{s}\|^2 / (\|\mathbf{s}\|^2 + k_2) \leq -\hat{\gamma} (|s_1| + |s_2| + |s_3| + |s_4|) \leq -\hat{\gamma} \|\mathbf{s}\| \quad (\text{A23})$$

where  $s_i$  is the  $i$ th component of  $\mathbf{s}$ . Employing the update law (Eq. 22) for the robust gain  $\hat{\gamma}$  and based on inequalities (Eqs. A22 and A23), Eq. (A21) can be expressed with some simplifications as

$$\dot{V} \leq -\lambda'' \mathbf{s}^T \mathbf{D}(\mathbf{q}) \mathbf{s} \quad (\text{A24})$$

Therefore, all signals appearing in the Lyapunov function remain bounded and consequently  $\mathbf{s} \in l_\infty$ . By integrating both sides of Eq. (A24), one can obtain:

$$\lambda'' \lambda_D \int_0^\infty (s_1^2 + s_2^2 + s_3^2 + s_4^2) dt \leq V(0) - V(\infty) \quad (\text{A25})$$

where  $\lambda_D > 0$  is the infimum of the minimum eigenvalue of  $\mathbf{D}(\mathbf{q})$ . Based on Eq. (A25), it is concluded that  $\mathbf{s} \in l_2$  and this together with  $\mathbf{s} \in l_\infty$  implies that  $\mathbf{s} \in l_2 \cap l_\infty$ . Based on Property 1 and due to the boundedness of signals in the closed-loop dynamics (Eq. A16),  $\dot{\mathbf{s}} \in l_\infty$ . Since  $\mathbf{s} \in l_2 \cap l_\infty$  and  $\dot{\mathbf{s}} \in l_\infty$ ; therefore,  $\lim_{t \rightarrow \infty} \mathbf{s} = 0$  (using the Barbalat lemma).<sup>47</sup> Since the first three components of  $\mathbf{s}$  in Eq. (18) are zero,

$$\frac{d}{dt} (\varphi - \varphi_m) + \lambda' (\varphi - \varphi_m) = s_4 \quad (\text{A26})$$

is the only nonzero component of  $\mathbf{s}$ . In fact, Eq. (A26) is a first-order differential equation whose input  $s_4$  is such that  $\lim_{t \rightarrow \infty} s_4 = 0$ . As long as  $\lambda' > 0$ ,  $\lim_{t \rightarrow \infty} \varphi - \varphi_m = 0$  [29], and this completes the proof.

## Appendix B: The model of ground reaction forces

The model of GRFs is adopted from [42, 48] with minor corrections in equations and parameters. Especially, the employed functions have been considerably smoothed to avoid chattering and/or model discontinuity issues. For GRF modeling, three places with equal distances are selected beneath the sound foot and ankle prosthesis (as shown in Fig. 2). Then, assuming that the  $i$ th place has the position of  $(x_i, y_i)$  with respect to the global reference frame, the normal and horizontal components of the contact forces are assumed as follows:

$$\begin{aligned} F_N &= (-K_G y_i - C_G (y_i) \dot{y}_i) 1(-y_i) \\ F_H &= -\mu(\dot{x}_i) F_N \text{sat}(10\dot{x}_i) \end{aligned} \quad (\text{B1})$$

in which the employed functions are given by

$$\begin{aligned} C_G(y_i) &= \begin{cases} C_{\max} y_i < -h \\ C_{\max} \left| \frac{3}{h^2} y_i^2 - \frac{2}{h^3} |y_i^3| \right| & -h \leq y_i \leq 0 \\ 0 & y_i > 0 \end{cases} \\ 1(y_i) &= \begin{cases} 0 & y_i < 0 \\ y_i^4 - 2 \left( \frac{1}{h_1^3} + h_1 \right) y_i^3 + \left( \frac{3}{h_1^2} + h_1^2 \right) y_i^2 & 0 \leq y_i \leq h_1 \\ 1 & y_i > h_1 \end{cases} \\ \mu(\dot{x}_i) &= (\mu_d - \mu_s) \tanh(\varepsilon_\mu \dot{x}_i) + \mu_s \end{aligned} \quad (\text{B2})$$

and “sat” in Eq. (B1) is the saturation function.<sup>29</sup> Also, the ground is assumed to be flat ( $Y = 0$ ).

